Enhancement of photomultiplier sensitivity with anti-reflective layers

2012 J. Phys. D: Appl. Phys. 45 055102

(http://iopscience.iop.org/0022-3727/45/5/055102)

IOP PUBLISHING JOURNAL OF PHYSICS D: APPLIED PHYSICS

J. Phys. D: Appl. Phys. **45** (2012) 055102 (9pp) doi:10.1088/0022-3727/45/5/055102

Enhancement of photomultiplier sensitivity with anti-reflective layers

Stuart William Harmer[1,3], **Peter David Townsend**[2] **and Nicholas John Bowring**[1]

[1] Sensing and Imaging Group, Department of Engineering and Technology, Manchester Metropolitan University, Manchester M1 5GD, UK

[2] Science and Technology, University of Sussex, Brighton BN1 9QH, UK

E-mail: swharmer@gmail.com

Received 16 November 2011, in final form 16 December 2011
Published 20 January 2012
Online at stacks.iop.org/JPhysD/45/055102

Abstract

Photomultipliers are fast, sensitive and low noise light detectors which operate across the ultraviolet–optical–near infra red region of the electromagnetic spectrum. Sensitivity is determined by the composition of the photocathode layer in which incident photons excite photoelectrons and the thickness of this layer. Incident light is partially reflected from and partially transmitted through the photocathode layer, which is typically ∼20 nm thick, and this energy is unavailable for photoelectron excitation, limiting sensitivity. Typical reflectance and transmittance values at 500 nm are 21% and 33%, respectively, for KCsSb; 27% and 24% for RbCsSb and 36% and 35% for $Na_2SbK:Cs$. These substantial losses can be reduced by the addition of one or more transparent impedance matching layers between the photomultiplier tube (PMT) window and the photocathode, resulting in enhanced sensitivity without effecting the PMT geometry, photocathode deposition process or altering the acceptance angle of the photomultiplier. The impedance matching serves to reduce reflectance losses, increasing cathode absorptance. By using published measurements of the dispersive properties of bialkali and trialkali (S20) photocathode compositions, accurate modelling of the electromagnetic field distribution within the photocathode layer is possible. This model facilitates the prediction of the enhancement of sensitivity obtainable with an anti-reflective layer of zirconium dioxide (zirconia). The authors present the enhancement factors possible with standard bialkali and trialkali photocathode compositions using the material zirconia for impedance matching. Enhancement factors up to 27% and 38% are predicted for KCsSb and RbCsSb photocathodes, respectively, while an enhancement factor of up to 44% is predicted for the S20 photocathode.

1. Background

Photomultiplier tubes (PMTs) are the detector of choice for applications that require low noise, high sensitivity and short response time measurements. PMTs are particularly suited to photon counting applications and much use is made of them in scintillators for detection of nuclear radiation, particle physics experiments and in medical apparatus, including the recent advances in optical biopsy. In these applications semiconductor photodiode devices have still not displaced the venerable PMT and considerable advancement in photodiode technology will be required before this occurs. However, despite the continued importance of this optoelectronic device there has been only a slow improvement in the performance of the commercially available PMTs in the last 50 years [1]. Reasons for reduced efficiency arise from signal losses of reflection from the photocathode material and transmission through it, as well failures to convert absorbed photons into electron emission into the vacuum chamber. One factor causing inefficient use of light incident on the PMT is inherently due to the mismatch of permittivity between the photocathode and the surrounding media: the glass window of the PMT and the vacuum that exists inside the tube. Proposed methods that increase the absorptance, the fraction of the incident power that is absorbed within the photocathode layer, have produced configurations that enhance performance by

[3] Author to whom any correspondence should be addressed.

Table 1. A comparison of the overall quantum efficiency (QE), i.e. electrons emitted per incident photon, for commercial and recent experimental or modified PMTs. Values are selected for blue (400 nm) and red (800 nm) wavelengths.

PMT type	% QE blue	% QE red	Refs
Classic planar PMT designs	20–25	1–2.5	Most PMT manufacturers
Non-normal incidence, e.g. via prisms or structured surfaces	50	10	[1–5]
Highest values recently cited	~70	~14	[4]
Simple addition of an external reflector	~30	~3	[5]
Internal anti-reflective layers (e.g. BeO)	40–45		[6]

reducing the reflectance from the PMT window and reducing the transmittance through the photocathode layer. These techniques rely on controlling the angle that the incident light impinges upon the PMT window using additional optical elements, resulting in higher absorptance values than are achievable with normal or near normally incident light [1, 2]. Other methods propose the use of multiply reflecting structures, such as pyramids or cones, fabricated on the inside of the PMT window to reduce reflectance and enhance absorptance, or waveguiding within the tube window to enhance the overall absorption efficiency [3–5]. Such techniques can offer significant increases in sensitivity, but so far they have not been commercialized. There are also benefits from using additional thin film layers of suitable materials between the PMT window and the photocathode for better matching the impedance of the photocathode at optical frequencies. This can be achieved, resulting in less of the incident light being lost to reflection and transmission and more being absorbed within the photocathode layer [6]. This scheme, although not able to offer improvements on the scale achievable with the multi-pass and highly oblique configurations, can still provide a worthwhile performance increase without the undesirable requirement for additional optics. The anti-reflective layers are also compatible with production of very large scale PMT, as used for example in particle physics detectors. Table 1 offers a brief overview of performance gains from the attempts at structural redesigns and the current concepts. Note that there is considerable variability in the performance of commercial tubes, but the present approach should have value in all cases.

2. Impedance matching theory

For light that enters the PMT window the optical field incident upon the photocathode layer is partially reflected at the PMT window–photocathode interface due to the difference in the impedance of the photocathode layer to that of the PMT window. This effect is again evident for the optical field incident upon the photocathode–vacuum interface, where it is now the discrepancy between the impedance of the photocathode layer and that of free space that results in partial reflectance. The impedance is related to the

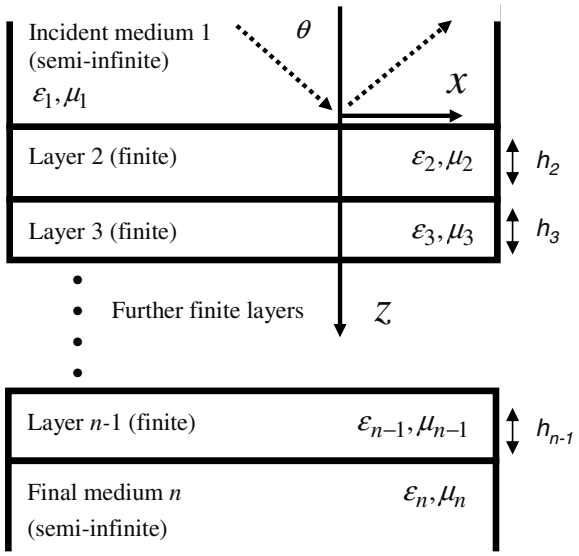

Figure 1. An illustration of the geometry of the model required for general analysis of a photocathode with one or more impedance matching layers. The y-direction is out of the plane of the paper.

complex permittivity and permeability of the medium and thus differences in these values result in partial reflectance of the optical fields at the boundaries between materials. A model that allows the prediction of the enhancement due to inclusion of one or more impedance matching layers will require analysing the system of layers displayed in figure 1.

We consider the allowed monochromatic, planar wave solutions to that can propagate in any of the layers, finite and semi-infinite. Plane waves are allowed here because the structure does not confine the waves in the x and y directions. This is a good approximation because the effects of diffraction from the edges of the PMT are negligible over the thickness of the PMT window and photocathode thickness. In the first case we consider only s-polarized light where the electric field is entirely parallel to the surfaces of the stack of media illustrated in figure 1. The electric field is, arbitrarily, chosen to exist in the y-direction only. The tangential components of the electric and magnetic fields in the jth layer are

$$ {}_yE_j = ({}_0E_{+j}\exp(\mathrm{i}\kappa_j z) + {}_0E_{+j}\exp(-\mathrm{i}\kappa_j z))\exp\mathrm{i}(k_x x - \omega t) \tag{1} $$

$$ {}_xH_j = \frac{-\kappa_j}{\mu_0\mu_j\omega}({}_0E_{+j}\exp(\mathrm{i}\kappa_j z) - {}_0E_{+j}\exp(-\mathrm{i}\kappa_j z))\exp\mathrm{i}(k_x x - \omega t) \tag{2} $$

where ${}_yE_{+,j}$ the y component of the complex electric field is vector and ${}_xH_j$ is the x component of the complex magnetic field vector. It is understood that the physical fields are represented by the real part of these expressions and of all other complex field quantities used in the following analysis. ${}_0E_{+,j}$ and ${}_0E_{-,j}$ are the complex electric field amplitudes of the positive and negative travelling waves, with respect to the z-axis, in the jth layer. The complex z component of the wave vector in the jth layer is given by κ_j, where $\kappa_j = k_0(\varepsilon_j\mu_j - \varepsilon_1\mu_1\sin^2\theta)^{1/2}$; $k_0 = 2\pi/\lambda$; $\omega = 2\pi\nu$; $c = \lambda\nu$ and $k_x = k_0\sqrt{\varepsilon_1\mu_1}\sin\theta$.

Here we use ν to denote the frequency of the radiation in cycles per second, λ to denote the wavelength of the radiation in free space and c is the speed of light in free space.

By imposing suitable boundary conditions on the electromagnetic fields given by equations (1) and (2), that of continuation of tangential components of the electric and magnetic fields across every interface, we have in the jth layer,

$$ {}_0E_{+,j}\exp(\mathrm{i}\kappa_j h_j) + {}_0E_{-,j}\exp(-\mathrm{i}\kappa_j h_j) = {}_0E_{+,j+1} + {}_0E_{-,j+1} \tag{3}$$

for the tangential electric field, and

$$\frac{\kappa_j}{\mu_j}({}_0E_{+,j}\exp(\mathrm{i}\kappa_j h_j) + {}_0E_{-,j}\exp(-\mathrm{i}\kappa_j h_j)) = \frac{\kappa_{j+1}}{\mu_{j+1}}({}_0E_{+,j+1} + {}_0E_{-,j+1}) \tag{4}$$

for the tangential magnetic field. Using equations (3) and (4) the complex electric field amplitudes for the positive and negative travelling waves in the $j+1$th layer can be written as a matrix equation in terms of the analogous quantities in the jth layer.

$$\begin{bmatrix} {}_0E_{+,j+1} \\ {}_0E_{-,j+1} \end{bmatrix} = \begin{bmatrix} (1+\chi_j)\exp(\mathrm{i}\kappa_j h_j) & (1-\chi_j)\exp(-\mathrm{i}\kappa_j h_j) \\ (1-\chi_j)\exp(\mathrm{i}\kappa_j h_j) & (1+\chi_j)\exp(-\mathrm{i}\kappa_j h_j) \end{bmatrix} \times \begin{bmatrix} {}_0E_{+,j} \\ {}_0E_{-,j} \end{bmatrix} \tag{5}$$

where $\chi_j = \kappa_j\mu_{j+1}/\kappa_{j+1}\mu_j = Z_{j+1}/Z_j$ is the ratio of the impedances in the $j+1$th layer and the jth layer.

Equation (5) is a recurrence relation which may be used to determine the complex electric field amplitudes in the jth layer in terms of the incident electric field amplitudes in medium 1. From equation (5) we obtain

$$F_j = M_{j-1}M_{j-2}\ldots M_1F_1 \tag{6}$$

where

$$F_j = \begin{bmatrix} {}_0E_{+j} \\ {}_0E_{-j} \end{bmatrix} \quad \text{and}$$

$$M_j = \begin{bmatrix} (1+\chi_j)\exp(\mathrm{i}\kappa_j h_j) & (1-\chi_j)\exp(-\mathrm{i}\kappa_j h_j) \\ (1-\chi_j)\exp(\mathrm{i}\kappa_j h_j) & (1+\chi_j)\exp(-\mathrm{i}\kappa_j h_j) \end{bmatrix}.$$

Since the product $M_{j-1}M_{j-2}\ldots M_1$ in equation (6) is itself a 2 by 2 matrix, we write for brevity,

$$N_j = M_{j-1}M_{j-2}\ldots M_1, \quad \text{where we define}$$

$$N_j = \begin{bmatrix} A_j & B_j \\ C_j & D_j \end{bmatrix}.$$

Equation (6) can now be written succinctly as

$$F_j = N_jF_1. \tag{7}$$

In the final semi-infinite medium, labelled by the index n in figure 1, there is no reflected wave as there is no discontinuity to partially reflect the transmitted wave, therefore from equation (7) we can write

$$\begin{bmatrix} {}_0E_{+n} \\ 0 \end{bmatrix} = \begin{bmatrix} A_j & B_j \\ C_j & D_j \end{bmatrix}\begin{bmatrix} {}_0E_{+1} \\ {}_0E_{-1} \end{bmatrix}. \tag{8}$$

Using equation (8) we can write the complex reflection and transmission coefficients for the electric fields from the layered structure. For the reflection coefficient we have

$$\Gamma_n = \frac{{}_0E_{-1}}{{}_0E_{+1}} = -\frac{C_n}{D_n}. \tag{9}$$

And for the transmission coefficient,

$$T_n = \frac{{}_0E_{+n}}{{}_0E_{+1}} = A_n - \frac{B_nC_n}{D_n}. \tag{10}$$

Using equations (1), (2) and (9) gives expressions for the EM field distribution in the jth layer in terms of the incident electric field amplitude, ${}_0E_{+1}$

$${}_yE_j = {}_0E_{+1}((A_j + B_j\Gamma_n)\exp(\mathrm{i}\kappa_j z) + (C_j + D_j\Gamma_n) \times \exp(-\mathrm{i}\kappa_j z))\exp\mathrm{i}(k_x x - \omega t) \tag{11}$$

$${}_xH_j = \frac{-\kappa_j{}_0E_{+1}}{\mu_0\mu_j\omega}((A_j + B_j\Gamma_n)\exp(\mathrm{i}\kappa_j z) - (C_j + D_j\Gamma_n) \times \exp(-\mathrm{i}\kappa_j z))\exp\mathrm{i}(k_x x - \omega t). \tag{12}$$

The irradiance I_j of the EM fields in the jth layer is given by the z component of the Poynting vector, averaged over a time cycle

$$I_j = -\frac{1}{2}\mathrm{Re}\{{}_yE_{j,x}H_j^*\}. \tag{13}$$

First we wish to find out the reflectance, transmittance and absorptance of the structure, these quantities are determined by the appropriate ratios of the irradiances in the two semi-infinite media.

The z component of the time-averaged Poynting vector for the incident EM wave is easily calculated using only the forward and backward travelling wave terms from equations (1) and (2) and applying equation (14).

$$I_{\pm1} = \sqrt{\frac{\varepsilon_1}{\mu_1}}\frac{|{}_0E_{\pm1}|^2}{2\mu_0 c}\cos(\theta). \tag{14}$$

The z component of the time-averaged Poynting vector in the final, semi-infinite medium is similarly evaluated

$$I_{+n} = \frac{|{}_0E_{+n}|^2}{2\mu_0 c|\mu_n|^2}(\mathrm{Re}\{(\varepsilon_n\mu_n - \varepsilon_1\mu_1\sin^2\theta)^{1/2}\}\mu_n' + \mathrm{Im}\{(\varepsilon_n\mu_n - \varepsilon_1\mu_1\sin^2\theta)^{1/2}\}\mu_n''). \tag{15}$$

The reflectance, transmittance and absorptance of the planar structure can be calculated from equations (14) and (15). The reflectance is given by

$$R = \frac{\langle I_{-1}\rangle}{\langle I_{+1}\rangle} = \left|\frac{{}_0E_{-1}}{{}_0E_{+1}}\right|^2 = |\Gamma_n|^2 = \left|\frac{C_n}{D_n}\right|^2. \tag{16}$$

The transmittance of the structure is defined as $T = \langle I_{+n}\rangle/\langle I_{+1}\rangle$ therefore the transmittance is:

$$T = \sqrt{\frac{\mu_1}{\varepsilon_1}}\frac{1}{|\mu_n|^2\cos\theta}\left|A_n - \frac{B_nC_n}{D_n}\right|^2 \times(\mathrm{Re}\{(\varepsilon_n\mu_n - \varepsilon_1\mu_1\sin^2\theta)^{1/2}\}\mu_n' + \mathrm{Im}\{(\varepsilon_n\mu_n - \varepsilon_1\mu_1\sin^2\theta)^{1/2}\}\mu_n''). \tag{17}$$

Finally, the absorptance of the *whole* structure is given simply by

$$A = 1 - (R + T). \tag{18}$$

Equation (13) can also be used to find the absorptance of individual layers, not just of the *whole* structure. The absorptance of individual layers making up the whole is calculated by considering the power flowing into and out of that individual layer divided by the power incident on the whole structure. This is important as some impedance matching layers may be slightly lossy and therefore the total absorptance cannot be used to predict performance gains. Note also that the overall quantum efficiency is influenced by the relative separation of the absorption site and the vacuum surface as photoexcited electrons need to travel through the layer and have sufficient energy to escape through the cathode/vacuum interface [1, 7]. By applying equations (11), (12), (13) and (14) we can find the absorptance of the jth layer, noting that the Poynting vector obtained from applying equation (13) to equations (11) and (12) will be a function of the distance z through the jth layer. The absorptance of the jth layer is simply

$$A_j = \frac{I_j(0) - I_j(h_j)}{I_{+1}(0)}. \tag{19}$$

The preceding analysis is valid only for s-polarized plane waves; the equations for p-polarized plane waves can be obtained directly from the equations for the s-polarized analysis with the following transformations applied.

$$E \to H; \qquad H \to -E \qquad \text{and} \qquad \varepsilon_j \varepsilon_0 \leftrightarrow \mu_j \mu_0.$$

Applying these transformations to the key results in the analysis, these being equations (16)–(19), gives the analogous equations for the p-polarized case. Under transformation the ratio of impedances given by χ_j is changed for p-polarization to $\chi_j = \kappa_j \varepsilon_{j+1}/\kappa_{j+1}\varepsilon_j$ this change in turn alters the elements A_j, B_j, C_j and D_j that form matrix N_j.

The EM fields for the p-polarized case are

$$\begin{aligned} {}_xH_j = {}&{}_0H_{+1}((A_j + B_j\Gamma_n)\exp(\mathrm{i}\kappa_j z) + (C_j + D_j\Gamma_n) \\ &\times \exp(-\mathrm{i}\kappa_j z))\exp \mathrm{i}(k_x x - \omega t) \end{aligned} \tag{20}$$

$$\begin{aligned} {}_xE_j = {}&\frac{\kappa_{j0}H_{+1}}{\varepsilon_0\varepsilon_j\omega}((A_j + B_j\Gamma_n)\exp(\mathrm{i}\kappa_j z) - (C_j + D_j\Gamma_n) \\ &\times \exp(-\mathrm{i}\kappa_j z))\exp \mathrm{i}(k_x x - \omega t) \end{aligned} \tag{21}$$

where ${}_0H_{+1}$ is the incident complex amplitude of the magnetic field. The reflectance for the p-polarized case is given by equation (16) with the modified matrix elements induced by changing χ_j.

The transmittance for the p-polarized case is

$$\begin{aligned} \mathrm{T} = {}&\sqrt{\frac{\varepsilon_1}{\mu_1}}\frac{1}{|\varepsilon_n|^2\cos\theta}\left|A_n - \frac{B_n C_n}{D_n}\right|^2 \\ &\times(\mathrm{Re}\{(\varepsilon_n\mu_n - \varepsilon_1\mu_1\sin^2\theta)^{1/2}\}\varepsilon_n' \\ &+\mathrm{Im}\{(\varepsilon_n\mu_n - \varepsilon_1\mu_1\sin^2\theta)^{1/2}\}\varepsilon_n''). \end{aligned} \tag{22}$$

The total absorptance and individual layer absorptance for p-polarized light are given by equations (18) and (19) where the reflectance and transmittance are substituted by the analagous p-polarized quantities for the case of total absorptance and where the EM fields are represented by equations (20) and (21) for individual layer absorptance.

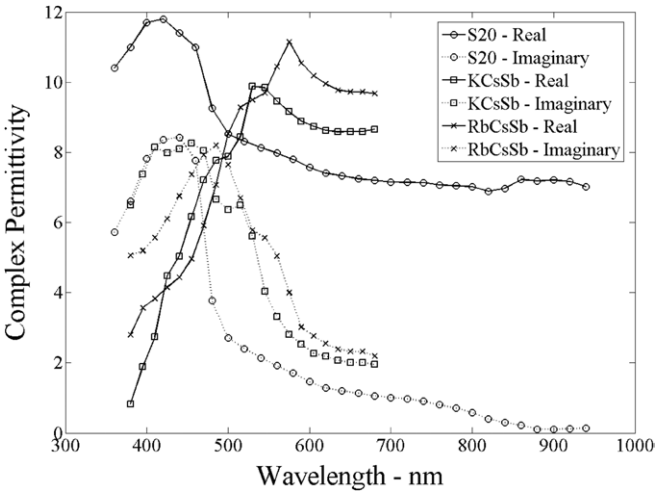

Figure 2. Dispersive data for the bialkali and S20 photocathodes compositions. The data for the bialkali are from Motta and Schonert [8], whilst those of the S20 cathode are from Hallensleben *et al* [2].

The glass window of the PMT has a thickness which is not controlled to sub-wavelength accuracy and therefore the interference from thin film effects in the glass layer needs to be averaged. If this is not done then spurious results will be obtained where constructive and destructive interference effects resulting from the precisely defined PMT window interfaces enhance or degrade absorptance in the photocathode layer. This effect is easily dealt with by noting that a complete cycle of interference (as measured by reflectance) takes place over a change in window thickness of

$$\Lambda = \frac{\lambda}{2\mathrm{Re}\{\sqrt{\varepsilon_2\mu_2 - \varepsilon_1\mu_1\sin^2\theta}\}} \tag{23}$$

where $\varepsilon_2\mu_2$ is the square of the refractive index of the window PMT window and $\varepsilon_1\mu_1 \approx 1$ for a PMT operating in air.

3. Results for bialkali photocathodes

The results from the mathematical analysis outlined in the previous section were implemented in the commercial software MATLAB. Comparison of performance between a PMT with and without impedance matching layers is simply quantified by the definition of enhancement factor. The enhancement factor is defined as the ratio of the photocathode absorptance, equation (19), with impedance matching layer(s) to the absorptance of the photocathode without any impedance matching layers (with the caveat that this might modify the depth profile of the absorption in the cathode). This metric well quantifies the expected improvement in performance as it can be shown that the addition of impedance matching layers does not alter the shape of EM field distribution within the photocathode, which is an important consideration for photocathode sensitivity [7], but only scales the amplitude of the EM field distribution within the layer. Thus enhancement

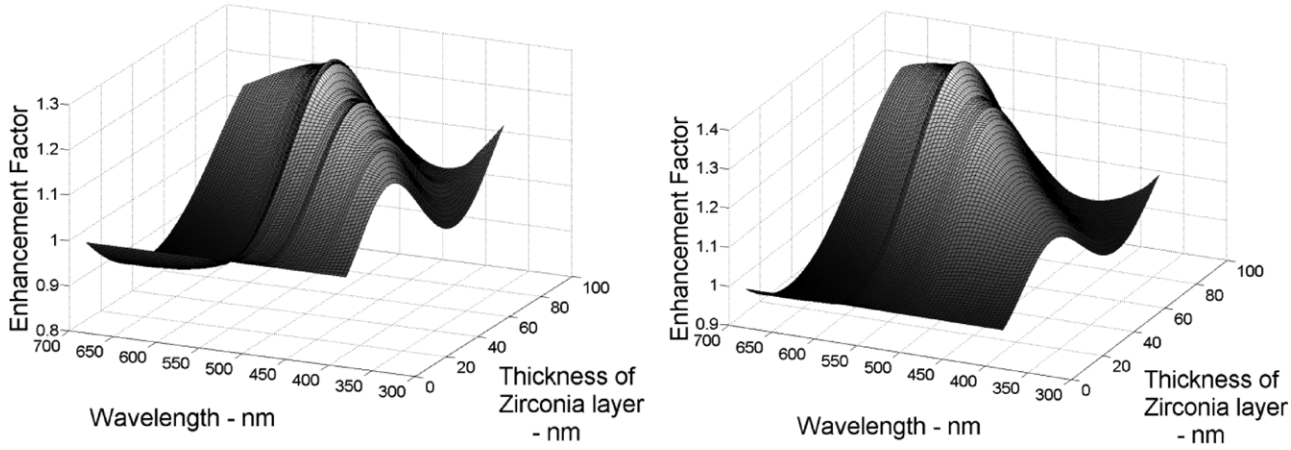

Figure 3. Predicted enhancement factors for typical thickness bialkali photocathode compositions: KCsSb of 20 nm (left) and RbCsSb of 25 nm (right). Enhancement factors of 27% for KCsSb and 38% for RbCsSb are realizable at wavelengths of 530 nm and 575 nm for ZrO_2 thickness values of 73 nm and 77 nm, respectively.

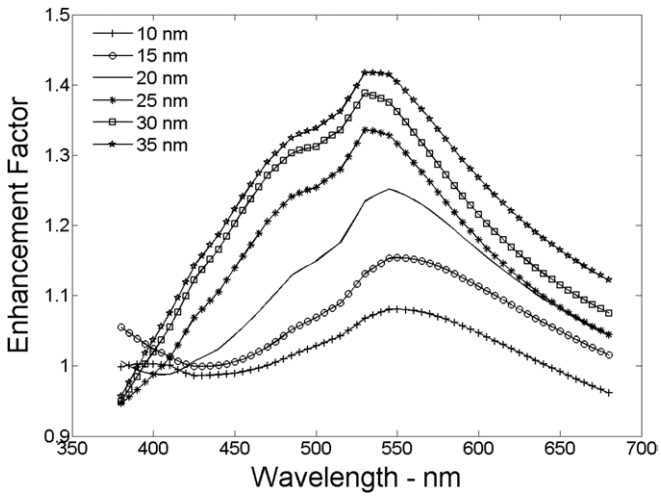

Figure 4. Enhancement factors predicted for the KCsSb bialkali cathode. The solutions have been optimized to give the highest mean enhancement across the wavelength range 380–680 nm, see table 1 for average values and required thickness of zirconia matching layers. The thickness without a marker is that measured by Motta and is representative of a typical KCsSb cathode thickness.

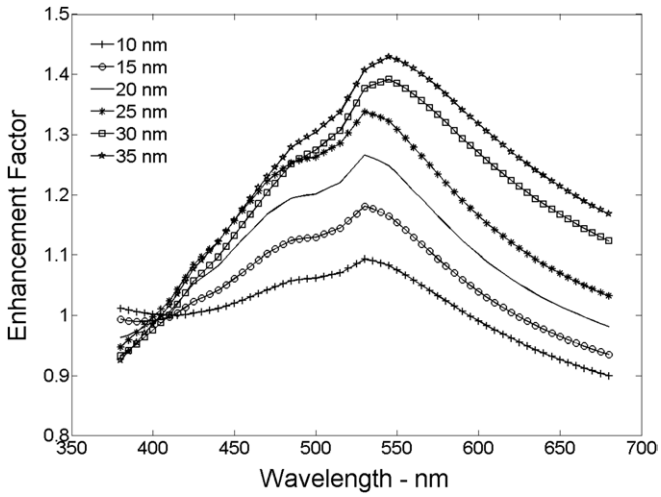

Figure 5. Enhancement factors predicted for the KCsSb bialkali cathode. The solutions have been optimized to give the highest global enhancement value within the wavelength range 380–680 nm, see table 1 required thickness of zirconia matching layers. The example for a 20 nm photocathode thickness (without markers) matches the data measured by Motta and is representative of a typical KCsSb cathode thickness.

of PMT performance should be directly proportional to the enhancement factor.

A suitable material must be chosen for the impedance matching layer. Suitability depends upon the material being chemically inert with respect to the highly reactive photocathode metals: potassium, sodium and caesium, and possessing appropriate dielectric properties to facilitate better impedance matching between the PMT window and photocathode. Multiple layers of different materials may be used to achieve impedance matching, the use of more than one layer can arise because several layers may provide a better impedance match than a single layer, in much the same way that high quality optics often have multiple coatings for anti-reflective purposes or that GRIN structures continuously vary the impedance over a spatial region to realize very highly anti-reflective structures (moth-eye, black silicon, etc). In this study the authors have only considered one layer impedance matching structures as these can provide very significant and worthwhile improvements without the associated costs of multiple layer coatings. The authors have selected zirconia for the purpose of impedance matching. Note this is not a unique choice and for example the Hamamatsu patent application [6] focuses on BeO for the bialkali tubes. Zirconia material has been selected here because it is transparent and near lossless over the wavelength region of interest (360–850 nm) and has a permittivity that is higher than that of the PMT window. Note that the refractive indices of PMT windows, such as silica or glass, are around ∼1.5 in the visible region. The variants of zirconia are higher at ∼2.19. All these values are much lower than the magnitude of the complex refractive index of the photocathode and therefore zirconia can provide a graded index structure. This may not only help us to reduce reflectance, but also increase absorptance.

Table 2. Optimized solutions for KCsSb.

Cathode thickness (nm)	Mean enhancement factor over 380–680 nm wavelength range	Optimum thickness of zirconia (nm)	Global maximum enhancement factor	Optimum thickness of zirconia (nm)	Wavelength of global maximum (nm)
10	2.1%	105	9%	92	530
15	7%	97	18%	81	530
20	**11%**	**84**	**27%**	**73**	**530**
25	16%	69	34%	67	530
30	20%	61	39%	68	545
35	24%	57	43%	63	545

Table 3. Optimized solutions for RbCsSb.

Cathode thickness (nm)	Mean enhancement factor over 380–680 nm wavelength range	Optimum thickness of zirconia (nm)	Global maximum enhancement factor	Optimum thickness of zirconia (nm)	Wavelength of global maximum (nm)
10	2.7%	100	10%	102	575
15	8%	90	20%	92	575
20	14%	79	29%	84	575
25	**19%**	**70**	**38%**	**77**	**575**
30	23%	63	44%	72	575
35	27%	58	48%	67	575

There are two standard bialkali photocathode compositions: KCsSb and RbCsSb, and the dispersive properties of these two bialkali compositions have been well documented [8, 9] and the data obtained from measurements by Motta and Schonert [8] are used here. The constants for the trialkali cathode (S20) have been documented by Hallensleben *et al* [2, 3, 10]. Figure 2 shows permittivity data for the three cathode types that are discussed here. We have assumed the thickness values obtained by Motta *et al* for the bialkali photocathode compositions KCsSb and RbCsSb of 20 nm and 23.4 nm, respectively, to be typical and so use a representative 'standard' thickness of 20 nm for the KCsSb cathode and 25 nm for the RbCsSb cathode.

Selection of the thickness of the zirconia layer used for impedance matching is of great importance as can be seen from the enhancement factor surfaces plotted in figure 3. We consider two optimization schemes: the first aims to optimize the enhancement factor over the wavelength range for which reliable permittivity data for the photocathode is available, this scheme is referred to as 'mean optimized'; the second optimization scheme considered finds the highest value of enhancement factor within the range of wavelengths where permittivity data exist. The first optimization scheme will lend itself to general improvements across the wavelength range 380–680 nm whereas the second optimization scheme will only provide large enhancement at a single wavelength and may well reduce performance at other wavelengths. For the two bialkali cathodes, both the mean and optimized enhancement schemes afford reasonable improvement over most of the wavelength range, see figures 4 and 5. The average enhancement factor predicted for a 20 nm thick KCsSb bialkali cathode optimized for mean enhancement is 11%; the same cathode can peak at 27% enhancement for global enhancement. The thicknesses of the zirconia matching layers required to achieve these enhancements are 84 nm and 73 nm, respectively, see table 2. Similarly, for the RbCsSb, with an additional zirconia layer thickness of 25 nm, the cathode can offer 19% mean enhancement and 38% global enhancement, see table 3.

Enhancement, using either optimization scheme, is sensitive to cathode thickness, and this is clearly visible in figures 4, 5, 6 and 7. With thicker cathode layers it is generally possible to gain greater enhancement factors; thinner cathodes respond with less enhancement. The addition of an anti-reflective layer will probably alter the optimum thickness of the cathode slightly, this is because the competing factors of absorptance and photoelectron transport are sensitive to the cathode thickness. Enhancement of the absorptance, for a given thickness of cathode, will leave the electron transport efficiency unaffected and will alter the balance between the competing factors of absorptance and electron transport. For very thick bialkali cathode layers the enhancement factors predicted are considerably greater than for standard thickness cathode layers suggesting that thicker cathodes are better improved by the addition of an anti-reflective layer, figures 4, 5, 6 and 7. Cathodes which are thinner than standard are less enhanced; therefore, this anti-reflective method of PMT enhancement will offer greater gains, over the untreated PMT, when applied to PMT that naturally require thicker cathodes (as is the case for some PMT optimized to work at longer wavelengths). The reason for this greater enhancement of thicker cathodes is the better impedance matching offered to the thicker cathode layer by the zirconia. A thin cathode appears to have an effective index which is lower than a thicker layer of the same material, altering the efficacy of the impedance matching offered by the zirconia layer. An anti-reflective layer of a material with a lower index might provide

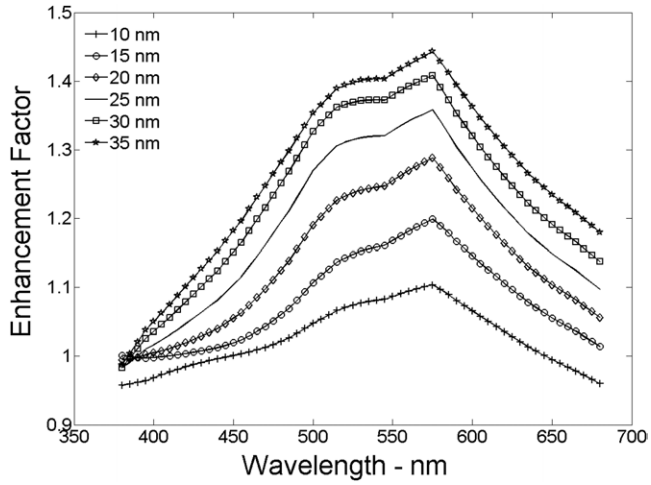

Figure 6. Enhancement factors predicted for the RbCsSb bialkali cathode. The solutions have been optimized to give the highest mean enhancement across the wavelength range 380–680 nm, see table 2 for average values and required thickness of zirconia matching layers. The 25 nm thickness calculation, without a marker, matches that measured by Motta and is representative of a typical KCsSb cathode thickness.

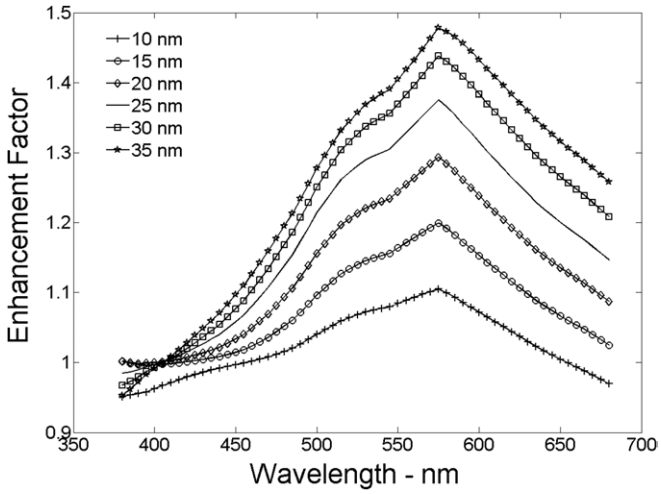

Figure 7. Enhancement factors predicted for the RbCsSb bialkali cathode. The solutions have been optimized to give the highest global enhancement value within the wavelength range 380–680 nm, see table 2 for required thickness of zirconia matching layers. The 25 nm thickness is representative of a typical RbCsSb cathode thickness.

better impedance matching for thinner cathodes and offer higher enhancement factors. Optimization of performance is reasonably insensitive to small changes (∼5 nm) in the thickness of the zirconia anti-reflective layer, the peaks for both bialkali cathode compositions in figure 3 are broad enough that a small error in zirconia thickness will not be catastrophic for performance. We reiterate that commercial production of cathodes is variable, but these current enhancements will still apply.

4. Results for trialkali (S20) photocathode

The $Na_2SbK:Cs$ trialkali (often termed S20) cathode is also very effectively enhanced by the addition of a suitably thick

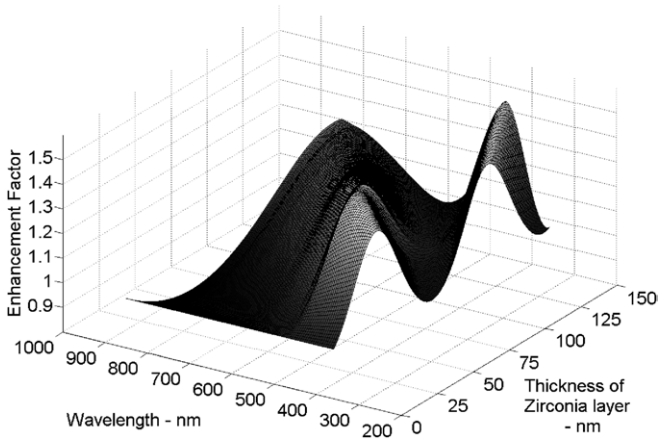

Figure 8. Predicted enhancement factors for the trialkali (S20) photocathode composition of typical thickness 35 nm [2]. A maximum enhancement factor of 45% is predicted at 460 nm for a ZrO_2 thickness of 45 nm.

zirconia layer, see figure 8. The persistence of high values of the complex permittivity to long wavelengths results in a second ridge in the enhancement factor surface, figure 8, which is not seen for the two bialkali cathode compositions, figure 3. The reason for this is that the wavelength range over which there is reliable complex permittivity data for the S20 [10] is considerably wider (360–850 nm as opposed to 380–680 nm). The extended wavelength range means the peak enhancement values occurring at shorter wavelengths can overlap, in cathode thickness space, the peak enhancement values at longer wavelengths (the enhancement factor is perfectly periodic in anti-reflective layer thickness space for a given wavelength, see equation (23)). In the case of the S20 cathode the mean optimization scheme averages across the wavelength range 360–850 nm, which is perhaps a rather large and unrealistically wide range to cover.

A mean enhancement factor of 17% is predicted for a standard (35 nm) thick S20 photocathode, requiring a 117 nm thick zirconia anti-reflective layer. Global enhancement of 44% is predicted at a wavelength of 460 nm for a 45 nm thick zirconia anti-reflective layer, see table 4. The mean enhancement and global enhancement schemes give considerably different curves for enhancement factor with wavelength, figures 9 and 10. This is in contrast to those for the bialkali cathode compositions where the shapes of the mean and global enhancement solutions with wavelength are similar, compared with figures 4, 5, 6 and 7. Again, the reason is the extended wavelength range over which the S20 cathode has been optimized; the global optimization scheme is unaffected by this but the mean optimization scheme is considerably influenced by the wavelength range, hence the significant differences observed between figures 9 and 10. With a standard thickness cathode (35 nm) significant enhancement factors are offered at shorter wavelengths, ∼400 nm, with a large dip occurring at ∼500 nm, with high enhancement again being predicted at longer wavelengths ∼700 nm, see figure 9. The global optimization scheme predicts significant enhancements only around the ∼450 nm wavelength region, see figure 10. Note that a key value of the S20 photocathode is red sensitivity,

Table 4. Optimized solutions for S20.

Cathode thickness (nm)	Mean enhancement factor over 360–850 nm wavelength range	Optimum thickness of zirconia (nm)	Global maximum enhancement factor	Optimum thickness of zirconia (nm)	Wavelength of global maximum (nm)
20	9.7%	131	*44%*	*46*	*400*
25	13%	127	*48%*	*42*	*400*
30	16%	122	*47%*	*41*	*420*
35	**17%**	**118**	***44%***	***45***	***460***
40	18%	112	*42%*	*50*	*490*
45	18%	100	*42%*	*59*	*540*
50	20%	69	*42%*	*62*	*575*

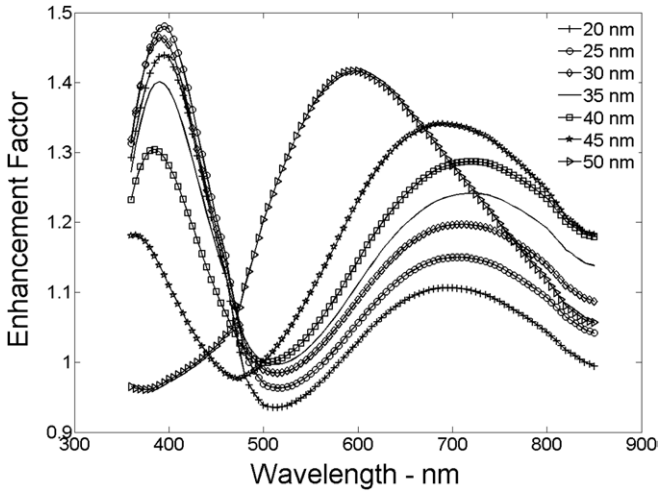

Figure 9. Enhancement factors predicted for different thicknesses of the S20 trialkali cathode. The solutions have been optimized to give the highest mean enhancement across the wavelength range 360–850 nm, see table 4 for average values and required thickness of zirconia matching layers. The thickness without a marker is that measured by Hallensleben and is representative of a typical S20 cathode thickness.

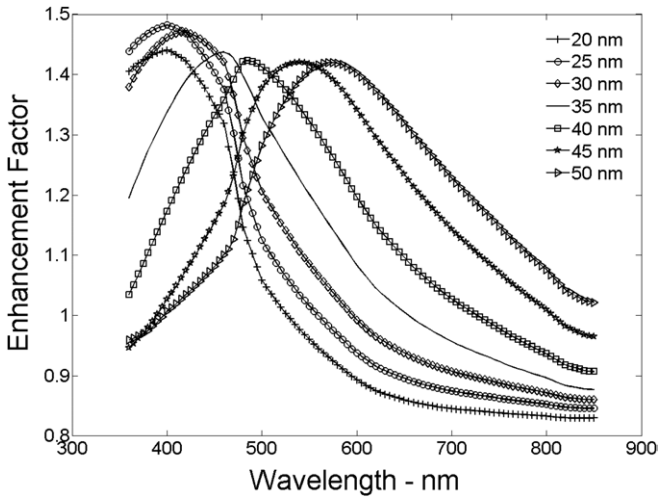

Figure 10. Enhancement factors predicted for various thicknesses of the S20 trialkali cathode. The solutions have been optimized to give the highest global enhancement value within the wavelength range 360–850 nm, see table 4 for the required thickness of zirconia matching layers. The thickness without a marker is that measured by Hallensleben and is representative of a typical S20 cathode thickness.

nevertheless this is always quite poor relative to the blue QE, and so any optimization of the S20 is likely to concentrate on the global optimization for long wavelengths.

As for the bialkali cathode compositions, the optimized solutions for the S20 cathode are relatively insensitive to thickness of zirconia; a small error or tolerance in the precision of the zirconia thickness layer will not drastically negate enhancement. This conclusion is evidenced by the rather broad, first peak featured in figure 8.

5. Summary

Significant performance enhancement of bialkali and trialkali photocathode compositions is predicted to be possible with the simple addition of an anti-reflective layer of zirconia between the PMT window and the photocathode layer. The enhancements are due to an increase in the absorptance of the photocathode which is caused by reducing the fraction of incident power which is reflected at the PMT window/photocathode interface, see figure 11. Optimization is by way of appropriate selection of the thickness of the zirconia anti-reflective layer, such that the increase in absorptance is achieved at a specific wavelength; over a specific wavelength range or simply gives the largest possible enhancement. The thickness of anti-reflective layer required for optimization at a specific wavelength is found by selecting the point of maximum enhancement factor at the desired wavelength from the relevant surface plot, see figures 3 and 8. Optimization over wide wavelength ranges is also possible by selection of a thickness of anti-reflective layer that provides the highest mean enhancement factor over the required range of wavelengths, in this case mean enhancement factors of 11%, 19% and 17% are predicted for KCsSb, RbCsSb and S20 photocathode compositions, respectively. Maximum global enhancement provides a measure of the largest improvement that can be expected using the zirconia anti-reflective layer for the three studied photocathode compositions; enhancement factors of 27%, 38% and 44% are predicted for KCsSb, RbCsSb and S20 photocathode compositions, respectively. Such increases in performance are interesting because of the relatively simple modification that is necessary. It is just the addition of a controlled thickness anti-reflective layer of zirconium dioxide prior to cathode deposition. This approach is applicable to the standard PMT as well as the very large area sensors used in particle physics. It is also

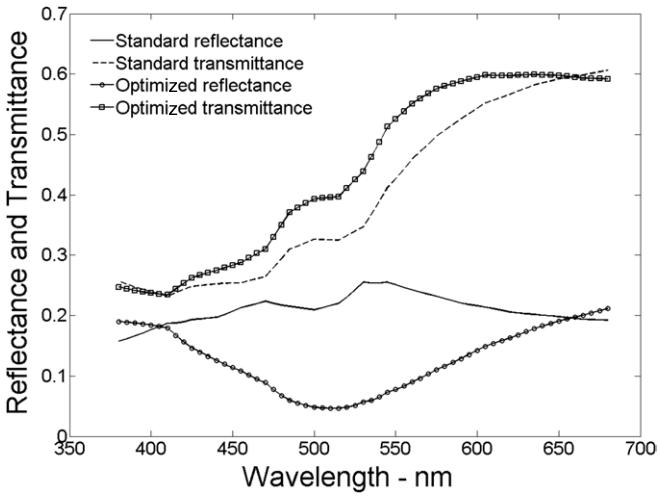

Figure 11. Example of how optimization, in this case of KCsSb bialkali cathode, with zirconia matching layer affects the reflectance and transmittance of the window and photocathode system. It is the reduction in reflectance of the system that accounts for the increase in absorptance and hence enhancement of performance. The transmittance is generally higher in the modified cathode than it is in the standard cathode.

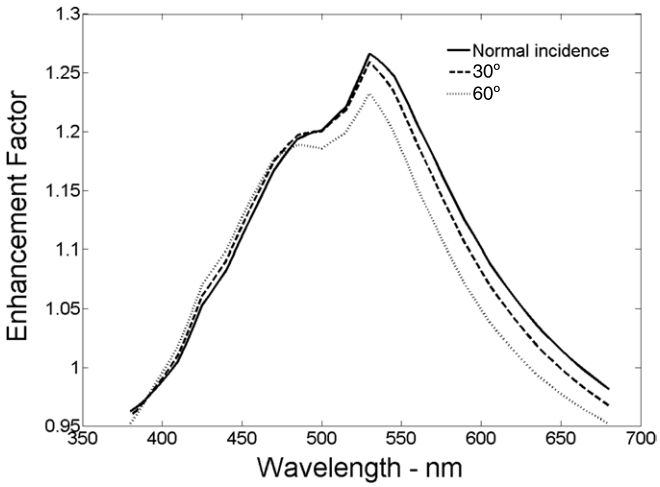

Figure 12. Example of sensitivity of enhancement factor to oblique incidence for the globally optimized solution of a 20 nm KCsSb bialkali cathode. The incident light is assumed to be unpolarized.

a valuable approach as it would still be compatible with the enhancement methods used in the structured photocathode designs, or those employing waveguide coupling, retaining the current PMT design geometry, collection angle and electron optics means the temporal characteristics (time of flight) of the PMT are not altered, so the modified PMT retains its widespread applicability and desirable properties. Another advantage is that the available enhancements are not highly sensitive to the thickness of the anti-reflective layer, meaning that very precise control and deposition of the anti-reflective layer is not required, see figures 3 and 8. The dependence of enhancement upon angle of incidence of light onto the PMT is also modest in the case of unpolarized light (as is the case for most applications). If the anti-reflective layer is optimized for best performance at normal incidence then a large change in incident angle still yields useful enhancement, see figure 12 for an example. This is valuable if one moves to the more powerful, but complex, enhancement techniques as summarized in table 1. The predicted enhancements are, however, subject to the cathode being accurately represented by the adopted model: a single homogeneous layer which can be characterized by an isotropic complex permittivity. There is some doubt on the accuracy of this assumption, as for the trialkali composition of photocathode significant deviation in complex permittivity has been measured [10] which could be due to varying stoichiometry of the cathode through the cathode thickness. Similarly the predicted enhancements are also reliant on the reproducibility of the cathode complex permittivity from sample to sample. If there is a wide variation in the complex permittivity, even if the situation is adequately described by a single cathode layer model, from tube to tube then optimization by correct choice of zirconia layer thickness cannot be made. Again, considerable variation has been noted in the trialkali photocathode [10]. We therefore conclude that an anti-reflective approach to the enhancement of PMT performance yields very worthwhile improvement with no obvious drawbacks apart from the slight extra complexity afforded in construction and the requirement that the photocathode complex permittivity is reasonably reproducible. In applications where every per cent of quantum efficiency is important such small disadvantages will be worth accepting for the boost in performance that is predicted.

References

[1] Townsend P D 2003 *Contemp. Phys.* **44** 17
[2] Hallensleben S, Harmer S W and Townsend P D 2000 *Opt. Commun.* **180** 89
[3] Townsend P D, Downey R, Harmer S W, Wang Y, Cormack A, McAlpine R and Bauer T 2006 *J. Phys. D: Appl. Phys.* **39** 1525
[4] Townsend P D, Valberg L, Momchilov N, Harmer S W, Downey R and Cormack A J 2008 *J. Phys. D: Appl. Phys.* **41** 185504
[5] Harmer S W and Townsend P D 2010 *J. Phys. D: Appl. Phys.* **43** 415101
[6] Watase F, Yamashita S and Watanabe H 2007 *European Patent* application EP 1939917A2
[7] Harmer S W and Townsend P D 2003 *J. Phys. D: Appl. Phys.* **36** 1477
[8] Motta D and Schonert S 2005 *Nucl. Instrum. Methods* A **539** 217
[9] Moorhead M E and Tanner N W 1996 *Nucl. Instrum. Methods* A **378** 162
[10] Harmer S W, Downey R, Wang Y and Townsend P D 2006 *Nucl. Instrum. Methods* A **564** 439